Role of Mo in the local configuration and structure stabilization of amorphous steels, a Synchrotron X-ray diffraction and Mössbauer study

E. Pineda [a,*], P. Bruna [b], J. Serrano [b,c], J. Torrens-Serra [d], D. Crespo [b]

[a] Departament de Física i Enginyeria Nuclear, ESAB, Universitat Politècnica de Catalunya, Esteve Terradas 8, 08860 Castelldefels, Spain
[b] Departament de Física Aplicada, EPSC, Universitat Politècnica de Catalunya, Avda. del Canal Olímpic s/n, 08860 Castelldefels, Spain
[c] Institució Catalana de Recerca i Estudis Avançats, Catalonia, Spain
[d] Grup de Nanomaterials i Microsistemes, Departament de Física, Universitat Autònoma de Barcelona. Edifici Cc, 08193 Bellaterra. Spain

ARTICLE INFO

ABSTRACT

Amorphous steels are promising materials with potential structural applications. The glass-forming ability (GFA) and mechanical properties of metallic glasses are intimately related to the local structure. In Fe-based alloys, Cr and Mo content seem to play a key role in stabilizing the amorphous atomic-level structure. Here we present a study on the effects of changing Mo content in $Fe_{72-x}C_7Si_{3.3}B_{5.5}P_{8.7}Cr_{2.3}Al_2Mo_x$ amorphous steels. We study the local structure of these alloys by Synchrotron X-ray diffraction and Mössbauer spectroscopy. The results show how the amorphous phase evolves from a ferromagnetic Fe-rich structure to a structure with predominance of paramagnetic environments with the increase of Mo content. The changes in the distribution of magnetic environments cannot be attributed only to the Fe–Mo substitution but to a change of local configuration in the amorphous phase.

© 2011 Elsevier B.V. All rights reserved.

1. Introduction

Small changes in composition of metallic-glasses (MG) may produce significant changes of their glass-forming ability and their physical and engineering properties such as strength, ductility or corrosion resistance [1]. At the atomic level, the stability of the metallic melt against crystallization is related to diverse factors. In some cases, the minor addition of some element modifies the 'rigidity' of the liquid structure either by changing the atomic packing efficiency or by generating strong bonds with other elements. In this way viscosity is increased and mobility at the atomic scale is reduced, slowing down the required atomic reconfiguration for crystallization. High GFA can also be related to a complex crystallization route or to crystalline phases with short range order quite dissimilar to the liquid structure [2,3].

This work analyses the effect of varying Mo content in amorphous alloys of composition $Fe_{71.2-x}C_7Si_{3.3}B_{5.5}P_{8.7}Cr_{2.3}Al_{2.0}Mo_x$ ($x = 0, 4.5, 6.5$ at.%). Fe-based bulk metallic glasses are often referred to as amorphous steels and they show exceptional values of strength and hardness in comparison to conventional, that is crystalline, steels. In this family of glassy alloys, the increase of GFA is often related to the destabilizing of α-Fe and the

appearance of more complex crystalline structure as a product of the first crystallization process [4]. Hirata et al. [5] studied the $Fe_{48}Cr_{15}Mo_{14}C_{15}B_6Tm_2$ crystallization process at a nanoscale level, concluding that the high thermal stability of the supercooled liquid is promoted by a rather complex crystallization process: amorphous → long period structure → χ-FeCrMo phase → $(Fe,Mo)_{23}C_6$. The latter phase has a unit cell of 116 atoms and the crystallization process involves the ordering of large regions of the amorphous structure.

The role of Cr and Mo in amorphous steels has been described as stabilizers of the amorphous phase. Their large negative heat of mixing with B, Si and P is expected to generate strong bonds within the amorphous structure, thus reducing the atomic mobility of the supercooled liquid. For the $Fe_{72-x}Mo_xY_6B_{22}$ system, Huang et al. [6] found that the addition of a proper amount of Mo increases the critical size of the amorphous cast rods from 2 to 6 mm. They attribute this effect to the creation of atomic arrangements with higher packing efficiency promoted by the differences in atomic size between Mo and the other elements.

The $Fe_{71.2-x}C_{7.0}Si_{3.3}B_{5.5}P_{8.7}Cr_{2.3}Al_{2.0}Mo_x$ alloys studied in this work have the particularity of being able to be prepared using industrial ferro-alloys, this reducing the cost of production [7]. In this work, however, the alloys were prepared using pure elements as will be detailed below. The changes in GFA due to Mo addition were investigated by Li et al. [8], they found that 4.5 at.% of Mo optimizes GFA this allowing them to produce completely amorphous rods with a maximum critical diameter of 6 mm.
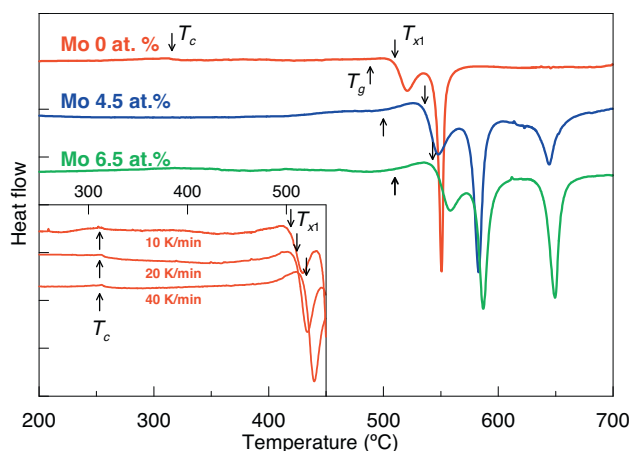
Fig. 1. DSC curves of Mo0, Mo4.5 and Mo6.5 ribbons obtained at a heating rate of 20 °C/min. (Inset) DSC curves of Mo0 obtained at 10, 20 and 40 K/min.

2. Materials and methods

Alloys with the adequate compositions were prepared by arc melting of pure elements, they were subsequently re-melted in an induction furnace and rapidly quenched in by melt spinning with a wheel velocity of 40 m/s under argon atmosphere. The obtained ribbon shape samples were 1 mm wide and 25 μm thick. EDX composition analysis of the rapid-quenched ribbons showed agreement with the expected composition within the experimental error. In the following, the three compositions studied in this work will be named as Mo0, Mo4.5 and Mo6.5, referring to their atomic content of Mo. The amorphous structure of the melt-spun ribbons was checked by X-ray diffraction (XRD). Differential scanning calorimetry (DSC) at 20 K/min was used to determine the glass transition and crystallization temperatures in a Perkin-Elmer DSC7. The local order around Fe atoms was investigated by transmission room temperature Mössbauer spectrometry (TMS) carried out under conventional conditions using a source of ^{57}Co in a Rh matrix; experimental spectra were fitted with Brand's NORMOS program [9] using a unique hyperfine field distribution (0–35 T). In situ XRD measurements during annealing were performed at the BM16 beam line of the European Synchrotron Radiation Facility with radiation energy of 15 keV. The ribbons were cut in 1 cm pieces and introduced into a Linkam hot stage, fixed in a ceramic washer. The diffracted intensity was collected by a 2-dimensional ADSC Q210r CCD detector perpendicular to the incident beam in transmission geometry. The ribbons were annealed from ambient temperature to 600 °C at a heating rate of 10 K/min. Spectra were acquired every 8 s allowing us to follow the structural changes of the samples throughout the process.

3. Results and discussion

As it is already known all three compositions are good glass-formers, Mo4.5 being expected to show the highest GFA. The other
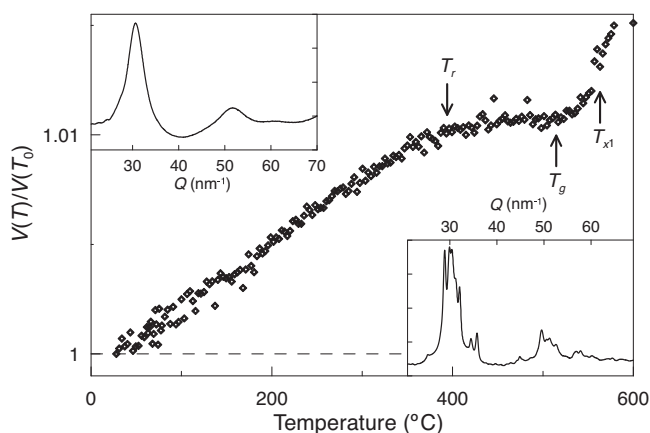

Fig. 2. Relative change of specific volume vs. temperature computed from the change in Q_{max} during in situ X-ray diffraction while annealing Mo6.5 sample. Top inset: diffraction pattern of the as-quenched alloy. Bottom inset: diffraction pattern of the alloy at 600 °C.
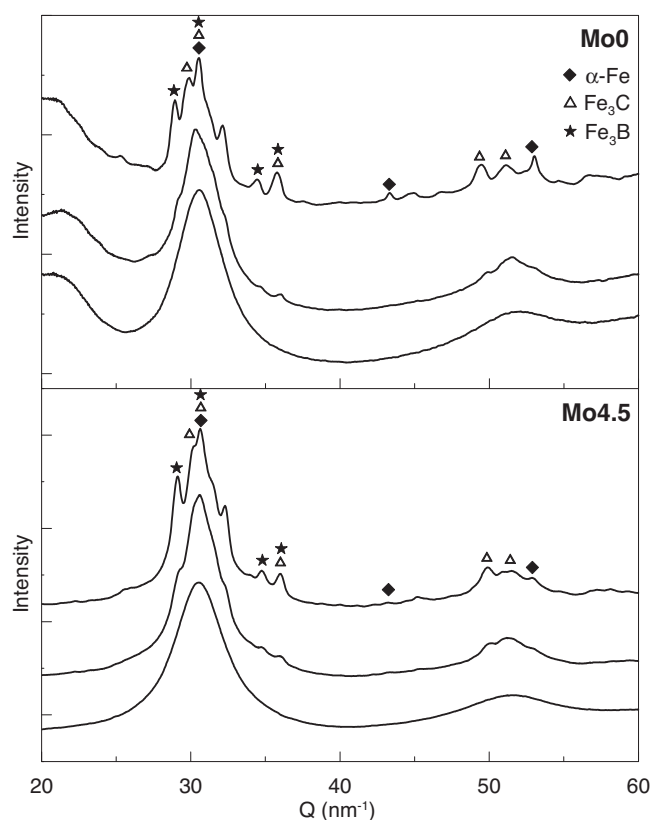

Fig. 3. X-ray diffraction intensity of Mo0 and Mo4.5 samples at three different temperatures. (Going from bottom to top) Mo4.5: $T_1 = 488$ °C, $T_2 = 580$ °C and $T_3 = 600$ °C, Mo0: $T_1 = 488$ °C, $T_2 = 550$ °C and $T_3 = 600$ °C.

two compositions – with Mo content $x = 0$ and $x = 6.5$ – correspond to the limits of the composition range previously studied by Li et al. [8]. A first-sight inspection shows that the Mo0 samples are tougher than the others; while the melt-spun Mo0 ribbons show resistance to being cut, the Mo4.5 and Mo6.5 compositions produce more brittle ribbons which split easily under manipulation.

DSC results in Fig. 1 show an increase of glass transition, T_g, and crystallization temperature, T_{x1}. In Mo0 samples, a Curie temperature T_c is clearly observed showing a ferromagnetic behaviour at room temperature. The inset in Fig. 1 shows the calorimetric signal of Mo0 ribbons for three different heating rates where T_c remains at constant temperature while glass transition and crystallization are shifted to higher temperatures as expected for kinetically controlled processes. A slight signal of a Curie transition is also found for Mo4.5 but it does not appear in Mo6.5. Temperatures T_g and T_{x1} increase with Mo content, as it is expected when adding elements of this same chemical group (Cr, Mo, W). Also the elastic constants and rigidity of the material are expected to increase thus explaining the increase in brittleness with Mo content. Characteristic temperatures of the three alloys are quoted in Table 1.

From DSC results, the better GFA of Mo4.5 can be ascribed to two effects. On the one hand the glass transition span, $\Delta T = T_{g,end} - T_{g,onset}$, becomes wider when adding Mo. This indicates

Table 1
Characteristic temperatures of the alloys obtained by DSC and X-ray diffraction.

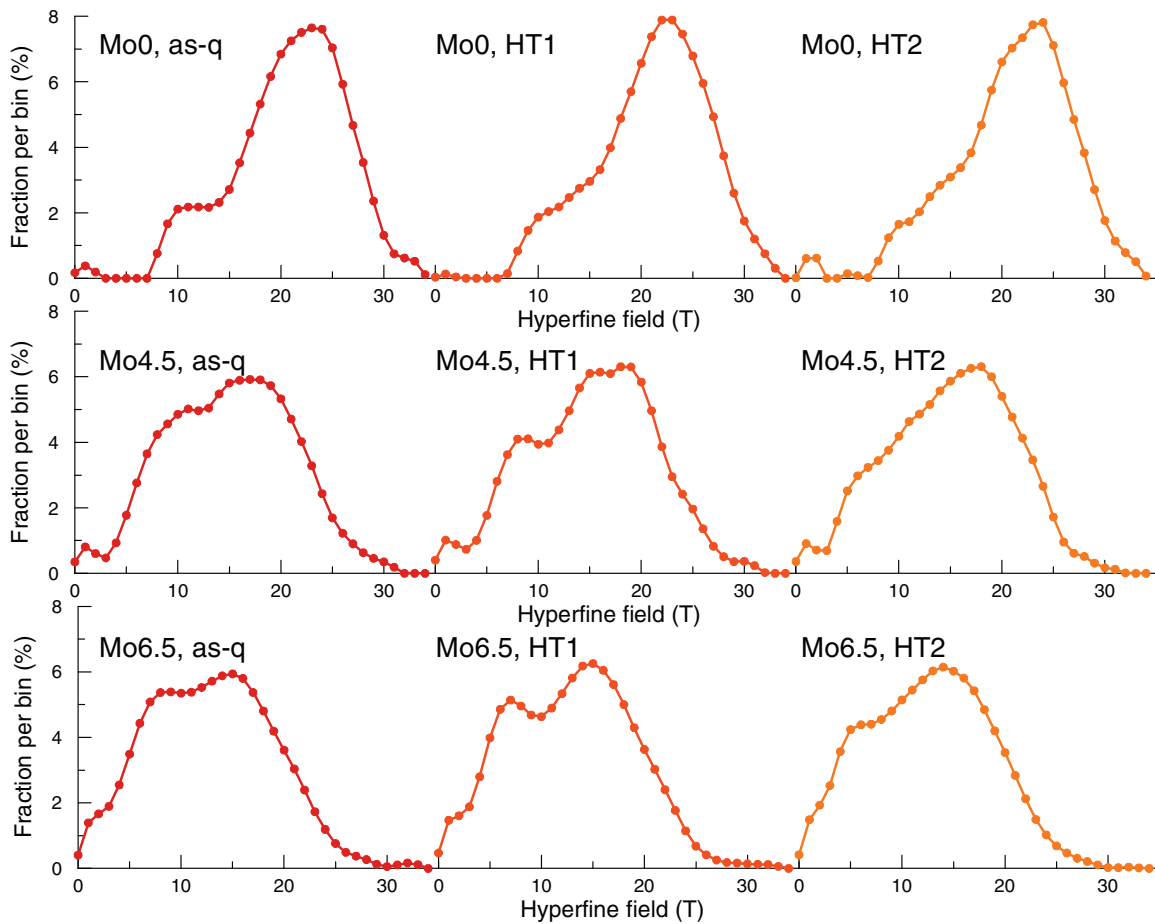| Alloy	DSC at 20 °C/min (°C)			XRD at 10 °C/min		
	T_c	$T_{g,onset}$	$T_{g,end}$	T_{x1} (°C)	T_r	T_g
Mo0	312 (1)	485 (1)	496 (1)	510 (1)	375 (2)	480 (2)
Mo4.5	175 (5)	503 (1)	520 (1)	535 (1)	410 (2)	513 (2)
Mo6.5	–	512 (1)	530 (1)	545 (1)	440 (2)	515 (2)

Fig. 4. Distributions of hyperfine fields around Fe-atoms obtained from Mössbauer spectroscopy of Mo0, Mo4.5 and Mo6.5 samples in the as-quenched state, slightly relaxed (HT1) and more deeply relaxed (HT2).

a slower decrease of the supercooled liquid viscosity over T_g, and so a more strong character of the liquid. On the other hand, the addition of Mo seems to trigger a third crystallization event which increases in intensity with Mo content. This crystallization process may limit the glass formability for high Mo contents when cooling form the melt.

Fig. 2 (top inset) shows X-ray diffracted intensity of the as-quenched Mo6.5 ribbons showing no signature of crystallization; very similar diffraction patterns were obtained for as-quenched Mo0 and Mo4.5. In an amorphous material the position of the main diffraction peak Q_{max} is not directly related to the average distance between atoms [10] but we can write

$$Q_{max} = \frac{2\pi K}{d},$$

where d is the distance between atoms and K depends on the particular amorphous configuration. This means that positions of main peaks can only be related to atomic distances for similar atomic arrangements. However, the studies realized up to now in metallic glasses show that the volume change inferred from Q_{max} using

$$\left[\frac{Q_{max}(T_0)}{Q_{max}(T)}\right]^3 = \frac{V(T)}{V(T_0)},$$

where $V(T)$ is the specific volume of the sample and T_0 is a reference temperature, is in accordance with macroscopic dilatometric measurements [11,12]. Fig. 2 shows the change in volume computed form $Q_{max}(T)$ while annealing at 10 K/min for Mo6.5; similar behaviour is observed for the other samples. The onset of structural relaxation and the glass transition are clearly identified by the

change in the thermal expansion coefficient in agreement with DSC results (see Table 1). Fig. 2 (bottom inset) shows the XRD pattern of the material at the final temperature of 600 °C.

The onset of crystallization is first observed in $Q_{max}(T)$ as an abrupt change or discontinuity, although the XRD patterns corresponding to such temperature does not show evidence of defined Bragg peaks. The small size of the crystals and the presence of remnant amorphous phase after the first crystallization process [8] results in broad and low Bragg peaks which are overlapped by the amorphous halo. However, they can be detected as soon as they produce a change in the maximum position of the pattern. Crystallization detected by sudden change of $Q_{max}(T)$ occur at temperatures near the crystallization onset observed in DSC signals while well defined crystalline peaks appear at much higher temperatures.

Fig. 3 shows the XRD patterns corresponding to Mo0 and Mo4.5 in a completely amorphous state, during crystallization and at $T = 600$ °C. In both compositions, the α-Iron phase Bragg peaks appear simultaneously with other phases (carbides and borides can be identified). The onset of the crystallization is found at higher temperatures for the alloys with Mo content, but the phases appearing as crystallization products seem to be the same, although α-Iron peaks are slightly more prominent in Mo0 than in Mo4.5 and Mo6.5 samples.

In Ref. [8] the authors performed TEM analysis of Mo0 and Mo4.5 compositions heated up to the end of the first crystallization process, this is up to the temperature between the first and second exothermic peaks observed in the DSC signal (Fig. 1). While only α-iron nanocrystals embedded in amorphous matrix were found

for Mo0, a combination of α-Iron nanocrystals with larger grains of other phases appeared when examining Mo4.5. Here we have obtained synchrotron XRD patterns throughout the whole crystallization including the two exothermic peaks. Considering Ref. [8] results, the first process is attributed to α-Iron nanocrystallization although it is hardly noticed in the XRD patterns where it is only detected by the sudden change in Q_{max}. The second process corresponds then to precipitation of carbides, borides and other unidentified phases, and it is evidenced by Bragg peaks in XRD patterns. The progressive overlapping of the two processes when increasing Mo content may explain the presence of other phases in TEM images of Mo4.5 heated samples in Ref. [8]. The crystalline phases precipitated during the third crystallization process at higher temperatures observed in Mo4.5 and Mo6.5 DSC signals have not yet been identified.

In order to evaluate the stability of the amorphous structure, the as-quenched samples were annealed with two different heat treatments. In the first one (HT1), the samples were annealed at 10 K/min up to the onset of the structural relaxation at 400 °C, while in the second treatment (HT2) they were annealed up to the glass transition temperature of each material allowing a deeper relaxation. Fig. 4 shows the hyperfine field distribution obtained from fitting the Mössbauer spectra. The as-quenched samples show a significant change of Fe-atoms environments due to Mo addition. This change cannot be ascribed to a mere substitution of Fe by Mo but to a change in the amorphous structure leading to a combination of at least two main Fe environments. All three samples show changes of the Fe-atom environments during structural relaxation. In Mo0 most of the Fe atoms are in an environment with an average hyperfine field similar to the one expected in ferromagnetic amorphous materials and also in a Fe_3B phase, the maximum of the distribution being at 23 T. Additionally to the main peak around the maximum it appears a second population of Fe-atoms in a paramagnetic environment at 10 T. The relaxation towards a more stable glassy phase is observed as a slight homogenization of the environments and an increase of the mean field, as it would be expected due to the densification occurred during relaxation. In Mo4.5 and Mo6.5 the maximum of the populations is found at 17 T and 15 T respectively and the second distribution peak at low fields increases with Mo content. The distribution of hyperfine fields in Mo6.5 shows two peaks with almost equal intensity. The structural relaxation is observed in the hyperfine field distribution as a two step process: (a) in HT1 annealed samples the population of Fe-atoms between the two peaks is shifted to high-field environments while the intensity of the low-field population remains almost constant and (b) in HT2 samples the reconfiguration to environments with higher fields continues but now is the population within the paramagnetic-like environment that diminishes significantly. The position of the maximum of the distribution in Mo4.5 and Mo6.5 indicates that Fe is surrounded by a configuration of neighboring Fe atoms with local hyperfine field similar to the one expected for a $(Fe,Mo)_{23}(C,B)_6$ structure (18 T). This phase is not observed as a product during the first stages of the crystallization but it is found in the samples crystallized during 15 min at 600 °C. In other amorphous steel compositions, high GFA has been attributed to an atomic order favoring crystallization of $(Fe,Mo)_{23}(C,B)_6$ instead of other less complex phases [5].

4. Conclusions

Structural changes during annealing of $Fe_{71.2-x}C_{7.0}Si_{3.3}B_{5.5}P_{8.7}Cr_{2.3}Al_{2.0}Mo_x$ ($x = 0$, 4.5 and 6.5) amorphous steels have been studied by Synchrotron X-ray diffraction and Mössbauer spectroscopy. The increase in Mo content shifts characteristic temperatures to higher values and increases brittleness. The relaxation and the first crystallization process have been studied by in situ X-ray diffraction measurements while annealing, showing the effects of structural relaxation and identifying the crystalline phases involved. An increasing Mo content increases the characteristic temperatures at which the crystallization events start, but does not alter significantly the crystalline phases appearing below 600 °C. The broadness of the crystalline peaks indicates a process with large nucleation of small crystallites, and a state still partially amorphous after the first crystallization process. The change of local Fe-environments during structural relaxation has been studied by Mössbauer spectroscopy. Owing to the superior glass-forming ability of Mo4.5 and Mo6.5, it may be inferred that the combination of two local environments (with low and high hyperfine field) induced by Mo addition benefits glass stability and inhibits crystallization differentiating the atomic configuration of the amorphous state from the competing crystalline phases.

References

[1] W.H. Wang, Prog. Mater. Sci. 52 (2007) 540–596.
[2] C. Fan, M. Imafuku, H. Kurokawa, A. Inoue, Scr. Mater. 44 (2001) 1993–1997.
[3] C. Fan, M. Imafuku, H. Kurokawa, A. Inoue, V. Haas, Appl. Phys. Lett. 79 (2001).
[4] A. Hirata, Y. Hirotsu, K. Amiya, N. Nishiyama, A. Inoue, Intermetallics 16 (2008) 491–497.
[5] A. Hirata, Y. Hirotsu, K. Amiya, A. Inoue, Phys. Rev. B 78 (2008) 144205.
[6] X.M. Huang, C.T. Chang, Z.Y. Chang, X.D. Wang, Q.P. Cao, B.L. Shen, A. Inoue, J.Z. Jiang, J. Alloys Compd. 460 (2008) 708–713.
[7] H. Li, S. Yi, Mater. Sci. Eng. A 449–451 (2007) 189–192.
[8] H.X. Li, K.B. Kim, S. Yi, Scr. Mater. 56 (2007) 1035–1038.
[9] R. Brand, L. Lauer, D. Herlach, J. Phys. F: Met. Phys. 14 (1984) 555.
[10] T.S. Hufnagel, R.T. Ott, J. Almer, Phys. Rev. B 73 (2006) 064204.
[11] A.R. Yavari, A. Le Moulec, A. Inoue, N. Nishiyama, N. Lupu, E. Matsubara, W.J. Botta, G. Vaughan, M. Di Michiel, A. Kvick, Acta Mater. 53 (2005) 1611–1619.
[12] D.V. Louzguine, A.R. Yavari, K. Ota, G. Vaughan, A. Inoue, J. Non-Cryst. Solids 351 (2005) 1639–1645.